Int. J. Electrochem. Sci., 15 **(2020)** 9049 – 9065, doi: 10.20964/2020.09.21

International Journal of ELECTROCHEMICAL SCIENCE
www.electrochemsci.org

Determination of the Gibbs Formation Energy of $CuGaSe_2$ by EMF Method

Muhsin Ider

Chemical Engineering Department, Faculty of Engineering, Usak University, Usak, 64200, Turkey
E-mail: muhsin.ider@usak.edu.tr

Received: 20 November 2019 / *Accepted:* 28 January 2020 / *Published:* 10 August 2020

The thermodynamic stability of the chalcopyrite $CuGaSe_2$ compound semiconductor was studied. A solid-state electrochemical cell was employed to obtain the standard Gibbs energy of formation of $CuGaSe_2$. The reversible EMF data of the following cell over the range of 818 to 950 K were measured: Pt, Ga(l), Ga_2O_3(s) // 15 YSZ // Ga_2O_3(s), Cu_2Se(s), $CuGaSe_2$(s), Cu, C, Pt. By using Cu_2Se literature data with the EMF results, the following expression for the standard Gibbs energy of formation for $CuGaSe_2$ was obtained: (ΔG^o_f $CuGaSe_2$) (kJ/mol) = -233.31 + 0.0075T(K) (818 to 950 K). The calculated ΔG^o_f function shows that the ternary $CuGaSe_2$ compound is more stable than the corresponding $CuInSe_2$ by approximately 10 kJ/mol over the entire temperature range of the present investigation, which is consistent with the current phase diagram information.

Keywords: $CuGaSe_2$, EMF, Gibbs energy of formation, enthalpy of formation, solid-state electrochemical cell.

1. INTRODUCTION

The ternary chalcopyrite compound semiconductors copper gallium selenide ($CuGaSe_2$) and copper indium selenide ($CuInSe_2$) are important ternary solar cell absorber materials. Copper indium gallium selenide (CIGS) is a tetrahedrally bonded chalcopyrite semiconductor that is a solid solution of $CuInSe_2$ (CIS) and $CuGaSe_2$ (CGS) with a chemical formula of $CuIn_xGa_{(1-x)}Se_2$ (CIGS), where the value of x can vary from zero to one. The thermodynamic and phase equilibrium data of $CuGaSe_2$ and $CuInSe_2$ are essential for CIGS-based solar cell manufacturing. However, the thermodynamics and phase equilibria of CGS are relatively less studied.

Due to the high absorption visible light coefficient of 10^4 cm^{-1} for CIS [1] and 2×10^5 cm^{-1} (500 nm) for CGS [2], thinner films of these materials are becoming more viable alternatives as sunlight absorbers. In addition, the direct band gap energy of 1.7 eV [3, 4] for $CuGaSe_2$ and 1.0 eV [4-6] for $CuInSe_2$ make CIGS-based bulk and epitaxial solar cell applications promising for research in

photovoltaic power systems. Gallium, sodium and sulfur addition in the structure in CIS-based solar cell device manufacturing processes shows advantages in band gap adjustment as well as prospects in other electronic properties such as defect chemistry and conductivity in semiconducting layers. This makes thermodynamic and chemical data of CGS more important for understanding diffusion and equilibrium parameters in thin film or bulk production processes. However, few critical assessments are available for CGS in the literature.

The compound $GuGaSe_2$ was first synthesized by Hahn [7]. Experimental data on the phase relations of the Cu-Ga-Se system as well as the pseudobinary section of the Cu_2Se-Ga_2Se_3 system exist in the literature. Most of the experimental data for phase equilibria are from differential thermal analysis (DTA) and X-ray diffraction (XRD) measurements [8, 9]. However, the thermochemistry of the Cu-Ga-Se system is relatively less studied, and considerable uncertainty still exists, especially for selenium-rich regions of the pseudobinary section of Cu_2Se-Ga_2Se_3. The literature data for pseudobinary sections of Cu_2Se-In_2Se_3 and Cu_2Se-Ga_2Se_3 systems show characteristic similarities. The thermodynamic data of the Cu-In-Se system were critically assessed by Ider [10], and the Gibbs energy of formation of $CuInSe_2$ was calculated from EMF measurements. The binary systems of Cu-Ga, Ga-Se and Cu-Se have already been assessed; however, the stability of ternary compounds and phase diagrams along the Cu_2Se and Ga_2Se_3 lines have not been critically assessed. Some of our preliminary EMF experiments for ternary compounds in Ga_2Se_3–rich composition ranges suggest that the pseudobinary section may be somewhat analogous to the Cu_2Se-In_2Se_3 system, which includes nonstoichiometric and large homogeneity range compounds. There is not much experimental information on the equilibrium nature of ternary compounds with the GaSe pseudobinary line.

Large homogeneous ranges of compounds of $Cu_1Ga_5Se_8$ and $Cu_1Ga_3Se_5$, which are analogous to CIS, have been reported [11-13]. The $Cu_1Ga_3Se_5$ structure is symbolized as the δ phase in the literature, which is shown in Fig. 1(a). It is assumed to be stable between 70 and 88% mole Ga_2Se_3 composition in the pseudobinary section of Cu_2Se-Ga_2Se_3. However, the stabilities of the ε-$Cu_1Ga_5Se_8$ and δ-$Cu_1Ga_3Se_5$ ternary compounds do not agree with the phase diagram information given in Fig. 1(b).

In general, there is not much thermodynamic transformation and Gibbs energy data on $Cu_xGa_ySe_z$ other than a few phase diagram studies and attempts to clearly determine and assess X-ray data except the standard enthalpy of formation $\Delta H^o_{f,298}$ [14] for β-$CuGaSe_2$. This creates reasonable ambiguity in phase equilibria and data optimization considering the difficulties in distinguishing large homogeneous range compound X-ray spectra with pertinent binaries. Hence, the present study is undertaken to determine the thermodynamic stability and formation Gibbs energy of $CuGaSe_2$ with the help of the solid oxide electrolyte EMF method. Additionally, the Gibbs energy function for $CuGaSe_2$ is estimated.

The ternary $CuGaSe_2$ compound crystallizes in a chalcopyrite structure, and the phase diagram of Cu-Ga-Se systems shows many characteristic similarities with other chalcopyrite I-II-VI_2 compounds. One of the most extended phase diagram studies was reported by Mikkelsen [8]. The phase diagram of the ternary Cu-Ga-Se system was studied by DTA and X-ray measurements. In addition to two ternary solid solutions that lie at the two edges of the Cu_2Se-Ga_2Se_3 pseudobinary line, only a chalcopyrite $CuGaSe_2$ solid solution was observed, which does not agree with some earlier interpretations of the δ solid solution phase extending between 71 mol% to 89 mol% Ga_2Se_3. The liquidus was found to include two regions of liquid immiscibility, one which extends from the Cu-rich immiscibility originating from

the Cu-Se binary to the Ga-rich immiscibility originating from the Ga-Se binary, and the other is related to the Se-rich immiscibility created by the Cu-Se binary phase region. X-ray powder diffraction patterns of samples quenched after annealing at 850 °C showed a single cubic phase with a nonlinear decrease in the lattice parameter from 78-100 mol% Ga_2Se_3. This result was interpreted as the existence of no two-phase regions at 850 °C. No reflection peaks were observed other than the peaks related to the zinc blende space group. However, it was also mentioned that three solid solutions were postulated for the analogous region of the Cu-Ga-S system, although it was not supported by X-ray analysis. The Ga_2Se_3-rich part of the constructed pseudobinary phase diagram was described with a zinc blended solid solution; however, no detailed explanation for the large value of Cu_2Se solubility in the Ga_2Se_3 phase was suggested.

Palatnik and Belova [9] studied the phase equilibria between 40 and 100 mol% Ga_2Se_3 along the quasi-binary section of Cu_2Se-Ga_2Se_3. No phase relations for the Cu_2Se-rich section were given. Numerous DTA data were interpreted to indicate that the chalcopyrite phase extended from 50 to 65 mol% Ga_2Se_3. A solid solution that is stable between 71 and 89 mol% Ga_2Se_3 was also reported. This compound, which was denoted by the symbol δ, can be represented by the chemical formula of $Cu_1Ga_3Se_5$. Another solid solution, which lies between 91 and 100 mol% Ga_2Se_3, is also reported and can be interpreted as $Cu_1Ga_5Se_8$, which is in disagreement with some of the earlier X-ray diffraction results. This phase is specified by the symbol ε in the phase diagram.

Bodnar and Bologa [15] reported that $CuInSe_2$ and $CuGaSe_2$, referring to A^I-B^{III}-C^{VI} compounds, crystallize in a chalcopyrite structure and are analogues to A^{II}-B^{VI} compounds. $CuInSe_2$ and $CuGaSe_2$ compounds and $CuIn_xGa_{1-x}Se_2$ solid solutions were synthesized from elements in double quartz ampoules in a vertical furnace. The compositions of the $CuInSe_2$ and $CuGaSe_2$ ternary compounds and the $CuIn_xGa_{1-x}Se_2$ solid solutions were tested by chemical analysis. The homogeneity and structure of the investigated compounds and solid solutions were determined by an X-ray method. The ternary compounds $CuInSe_2$ and $CuGaSe_2$ and the $CuIn_xGa_{1-x}Se_2$ solid solutions were found to crystallize in a chalcopyrite structure. The lattice parameters for $CuInSe_2$ ($a=5.782 \pm 0.002$ Å, $c=11.620 \pm 0.005$ Å) and $CuGaSe_2$ ($a=5.616 \pm 0.002$ Å, $c=11.016 \pm 0.005$ Å) are found to be close. The phase transformation temperatures were determined from DTA measurements. Annealed alumina was used as a reference material, and both heating and cooling measurements were performed. The thermal investigations showed two thermal transformation points for each ternary compound. $CuGaSe_2$ experienced phase transformations at 1045 and 1080 ºC, and $CuInSe_2$ experienced phase transformations at 810 and 986 ºC. Similar phase transformations were also found for solid solutions over the whole composition range. Bodnar and Bologa [15] summarized the experimental data measured along the $CuInSe_2$-$CuGaSe_2$ phase line in a figure. The phase transformation at 1045 ºC for $CuGaSe_2$ was assumed to be related to cation-cation disordering by an analogous assessment of Palatnik and Rogacheva [16] that referred to the phase transformation of $CuInSe_2$ at 810 ºC. The phase transformation temperature of 1045 ºC is consistent with the value of 1050±5 ºC by the earlier report of Palatnik and Belova [9], which is represented by the peritectic phase reaction.

Jitsukawa [17] investigated the pseudobinary phase diagrams of Cu_2Se-$CuGaSe_2$ and $CuSe$-$CuGaSe_2$ systems for single, high-quality crystal growth of $CuGaSe_2$. The single crystals were precipitated by the solution Bridgman method with nearly stoichiometric compositions. By using DTA

and XRD and an electron probe microanalyzer (EPMA), phase diagrams of Cu_2Se-$CuGaSe_2$ and CuSe-$CuGaSe_2$ pseudobinary systems were constructed. Then, the crystal growth of $CuGaSe_2$ was performed on the basis of measured phase diagram data. A better reaction path to grow large crystals was suggested to be the use of CuSe instead of Cu_2Se. The peritectic reaction temperature between the sphalerite + liquid phase to the chalcopyrite phase was found to be 1054 ºC, which is in very good agreement with earlier results. The eutectic line was determined from the DTA signal to be 996 ºC. The eutectic line, peritectic temperature and temperature of the liquidus line were approximately 20 ºC higher than the data of Mikkelsen [8]. In contrast, Palatnik and Belova [9] did not report a eutectic reaction between liquid and chalcopyrite-$CuGaSe_2$+Cu_2Se(ss), and their composition at the peritectic point also differs from the results of Jitsukawa [17]. The comparison of various experimental data measured along the pseudobinary of Cu_2Se-Ga_2Se_3 is given in Fig. 1(a) and Fig. 1(b).

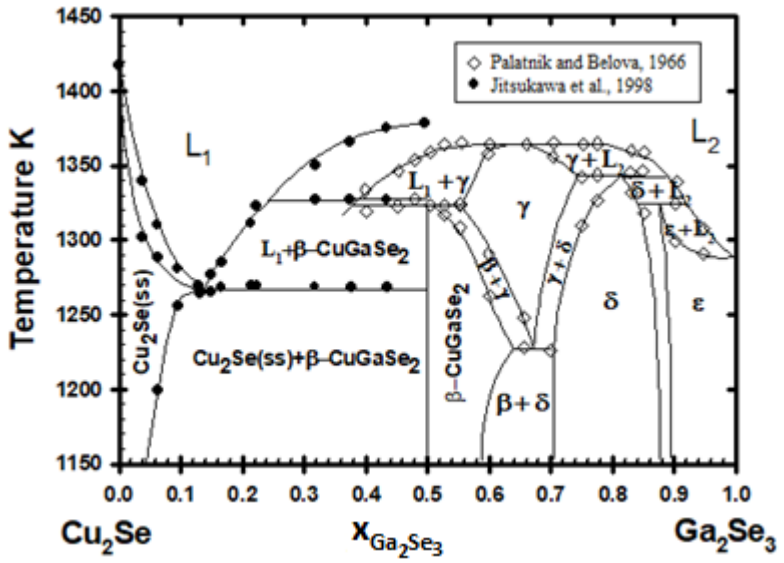

Figure 1. (a) Illustration of various experimental data along the Cu_2Se-Ga_2Se_3 pseudobinary by Palatnik and Belova [9] (Adapted from ref. [9], with permission. Copyright 2020 Nauka Publishing House) and Jitsukawa [17] (Adapted from ref. [17], with permission. Copyright 2020 Elsevier).

Matsuhita [18] investigated the chemical reaction processes forming a single phase in the $CuIn_xGa_{1-x}Se_2$ system, as well as the intermediate products, using DTA and powder X-ray diffraction. The $CuGaSe_2$ (x=0) and $CuInSe_2$ (x=1) compounds showed phase transition points at 1060 and 815 ºC, which is also consistent with earlier reports.

A few reports have been published on the effects of sodium on the efficiency of thin film Cu(In, Ga)Se_2 solar cells. However, there is no general conclusion on how the diffusion mechanism influences the defect chemistry and defect structure or electrical properties.

Tanaka [19] investigated whether sodium effects also occur in thin films containing In(Ga)-rich layers on the surface of the absorber layer of Cu(In,Ga)Se_2. Thin films of Cu(In, $Ga)_2Se_{3.5}$ were prepared by radio frequency sputtering from stoichiometric $CuIn_xGa_{1-x}Se_2$ (x=0.6) and Na_2Se mixture targets. The X-ray results showed that the lattice parameters of Cu:(In+Ga):Se=1:2:3.5 films were slightly smaller

than those of Cu(In, Ga)Se_2. In addition to the peaks appearing for chalcopyrite structure Cu(In, Ga)Se_2, an additional peak was observed. Similar sodium effects were found for In(Ga)-rich thin films. The optical band gap of the $Cu(In_{0.6}Ga_{0.4})Se_{3.5}$ thin film was found to be 1.36 eV, which is larger than 1.24 eV. Both p- and n-type conduction were observed.

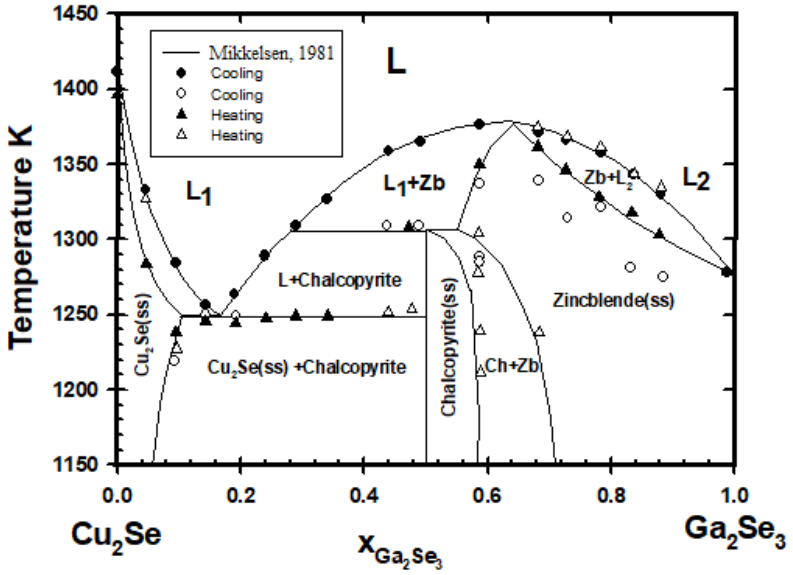

Figure 1. (b) Illustration of various experimental data along the Cu_2Se-Ga_2Se_3 pseudobinary by Mikkelsen [8] (Adapted from ref. [8], with permission. Copyright 2020 Springer Nature).

A few reports on the electrical and optical properties have been published. Schroeder [20] studied hole transport and doping states in epitaxial $CuIn_{1-x}Ga_xSe_2$. Temperature-dependent mobility, resistivity, and carrier concentration measurements were made on epitaxially grown single-crystal thin films of $CuIn_{1-x}Ga_xSe_2$ by a hybrid sputtering and evaporation process on GaAs substrates. A general discussion of the relationship between defects and deviation from stoichiometric compositions is presented. It was suggested that the lack of dependence on the I/III for I/III-rich samples proves that electrically active defects may not be responsible for deviations from stoichiometry in these materials.

A thermodynamic review was reported by Cahen [21] on the basis of literature data of thermodynamic quantities and functions for species that can be involved in the preparation of thin films of $CuInSe_2$. The free energies and enthalpies of the possible gas phase and surface reactions for the preparation of $CuInSe_2$ were studied. In addition, free energies and enthalpies of formation for I-III-VI_2 compounds and related binary data were also compiled. Calculated values for $\Delta G^o_{f,298}$= -313 kJ mol^{-1} and $\Delta H^o_{f,298}$= -316 kJ mol^{-1} were reported for $CuGaSe_2$. In this paper, some missing values were calculated from possible binary alloy reactions. At times, values for $\Delta H^o_{f,298}$ were estimated by considering binaries, I-III-VI_2 from (I_2VI+III_2-VI_3) or (I-VI+III-VI). However, the enthalpy of formation and Gibbs energy of formation data for $CuInSe_2$ and $CuGaSe_2$ were obtained only for 298 K. Gibbs energy functions with respect to temperature were not obtained due to limited data.

There is not much literature information on $\Delta H^{o}_{f,298}$ or $\Delta G^{o}_{f,298}$ for $Cu_1Ga_3Se_5$ and $Cu_1Ga_5Se_8$ compounds. The Gibbs energies of $CuGaSe_2$, $Cu_1Ga_3Se_5$ and $Cu_1Ga_5Se_8$ were not evaluated from phase diagram optimization due to uncertainty in the equilibrium data.

In this work, the $CuGaSe_2$ Gibbs energy of formation is first calculated from EMF measurements. The Gibbs energy of formation for $CuGaSe_2$ over the range of 818 to 950 K is obtained. Additionally, the Gibbs energy function of $CuGaSe_2$ is derived for the first time from EMF measurements, which is necessary in equilibrium calculations and phase diagram optimizations.

In the following section, the EMF measurements on $CuGaSe_2$ are explained. The derived Gibbs energy functions and calculated thermochemical data are presented in section 3. A comparison of the calculated values with selected Gibbs energy and enthalpy data is given in Tables 2 and 3.

2. EXPERIMENTAL

2.1. Materials and synthesis

High-purity Ga (99.9999 mass%, Johnson Matthey), Ga_2O_3 (99.99 mass%, Johnson Matthey), CuSe (purity greater than 99.5 mass%, Johnson Matthey, USA), GaSe and Cu_2Se (purity greater than 99.99 mass%, Johnson Matthey, USA) were used as the starting materials. The ternary compound $CuGaSe_2$ was synthesized by heating a mixture of CuSe and GaSe in a stoichiometric 1:1 mole ratio in a quartz ampoule. The ampoule was sealed under vacuum, which was kept at a pressure of equal or less than 10 Pa with a rotary pump. This quartz ampoule was heat treated in stages at 973 K for 94 hours, 1353 K for 71 hours, 1273 K for 95 hours, 1073 K for 47 hours, 973 K for 44 hours, followed by annealing at 873 K for 216 hours. This procedure was repeated at least twice to ensure the completeness of the reaction. The above temperatures and heat treatment sequences were determined by repeated exercises. The compound was taken from quartz ampoules and powdered for direct use in EMF cells. The powder XRD method was used to ensure the formation of the $CuGaSe_2$ compound. A Philips 3720 X-ray diffractometer was used for analysis. A mixture of $CuGaSe_2$ / Cu_2Se / Cu / Ga_2O_3 in equimolar ratio was compacted into pellets and heated to 1000 K in purified argon for 24 hours and checked for coexistence. The pellets were prepared by using a micro/macro 13-mm KBr die set (International Crystal Labs). A maximum force of 10 tons was applied on each sample by a hydraulic press.

2.2. EMF measurements

The test electrodes were made by intimately mixing powder Cu_2Se (purity greater than 99.99 mass%, Johnson Matthey, USA) and synthesized $CuGaSe_2$ powder with one third of their mass of Ga_2O_3. Pellets and powder mixtures for test electrodes were alternatively used. For pellet preparations, a maximum of 10 tons was applied on the coexisting phase mixtures by a hydraulic press. The pellet diameters were usually between 10 and 12 millimeters. The thicknesses of the pellets were usually less than 3 millimeters. The mixtures were usually allowed to equilibrate within the cell under a flow of a blanket gas for long startup times. Some excess copper (1Cu/1cell-Pellet, w/w) was added to the test electrodes to ensure stoichiometric coexistence of the compounds in the cell. The galvanic cell was

located at the most homogeneous temperature zone of the furnace, which is described in Fig. 2. The open cell structure setup shown in Fig. 3 was mostly used throughout the experiments.

The reference electrodes were prepared from a mixture of 4:1 weight ratios of high-purity Ga (99.9999 mass%, Johnson Matthey) shots and Ga_2O_3 (99.99 mass%, Johnson Matthey) powders. Pellet or powdered samples were used in reference electrodes. Electrode materials were allowed to equilibrate within the cell at the lowest temperature of measurement.

The following cell configuration over the range 818 to 950 K was studied:

Pt, Ga(l), Ga_2O_3(s) // YSZ // Ga_2O_3(s), Cu_2Se(s), $CuGaSe_2$(s), Cu, C, Pt I

where YSZ denotes 15 mass % yittria (Y_2O_3)-stabilized zirconia (ZrO_2). YSZ is a solid oxide electrolyte that is used as a solid O^{2-} (oxygen ion) ionic conductor at high temperatures, usually between 600-1100 °C. The symbol C denotes a high-density graphite cup that is used to hold the test electrode materials. Pt denotes platinum wire, which is used as the electric contact. Cylindrical YSZ crucibles with 15-mm diameter and 3-mm thickness were used in an open cell setup to hold the electrode materials. Specifically, nuclear-grade high-density graphite cups and alumina crucibles were employed to hold the test electrode materials. In the open cell arrangement, graphite and YSZ crucibles enclosing the test and reference electrodes were sealed with a magnesia-based high-temperature ceramic sealant (Aremco 571) to avoid vaporization of elements and leakage of electrode materials.

The absence of asymmetric potentials due to the graphite cup was tested by measuring almost null EMF (±1 mV) values in symmetrical cells with identical Ga(l)/Ga_2O_3(s) electrodes with graphite cups. A nearly null EMF was measured over the range of 800 to 1100 K, thereby showing the absence of significant errors arising from asymmetric potentials. The isothermal zone map of the furnace between 600 and 1000 °C was carefully determined by thermocouple readings before the experiments. During data acquisition, both electrodes were carefully located at the highest temperature and most isothermal zone of the furnace. This enabled the solid oxide ion conductor to be in its highest ionic conduction domain at both electrodes. It is noted that the ionic conductor has its highest ionic conductivity values at approximately 1000 °C. This causes electrochemical reactions to reach equilibrium more slowly below that temperature. The temperature range of the adopted measurements was high enough that there was no detrimental influence from partial electronic conduction.

The EMF system was purged repeatedly before each experiment. The system was filled with purified argon and evacuated to remove any residual oxygen and other impurities. During the measurements, a nearly static atmosphere of purified argon with a flow rate of less than 20 mm^3/minute flowed through the system to avoid any gas phase interaction between electrodes in cell compartments. The purified argon with a positive pressure difference was maintained throughout to prevent any oxygen back diffusion. The temperature of the cell was measured by using a Pt-10%Rh/Pt thermocouple whose junction was located near the electrodes of the cell in the isothermal zone of the furnace. The reversibility of the EMF readings was verified by the thermal cycling response as well as micropolarization. The test electrodes were examined by XRD at the end of each experiment to ensure the absence of phase changes or oxidation. Other experimental details, such as argon purification and voltage measurements, are explained elsewhere [22, 23]. However, a slight alteration from these experimental details was made by adding extra titanium sponge at the bottom of the alumina/quartz cylinder, as shown in Fig. 2. The

detailed experimental schematics for the EMF measurement system are given in Fig. 2. The description of cell arrangements for the EMF measurements is given in Fig. 3.

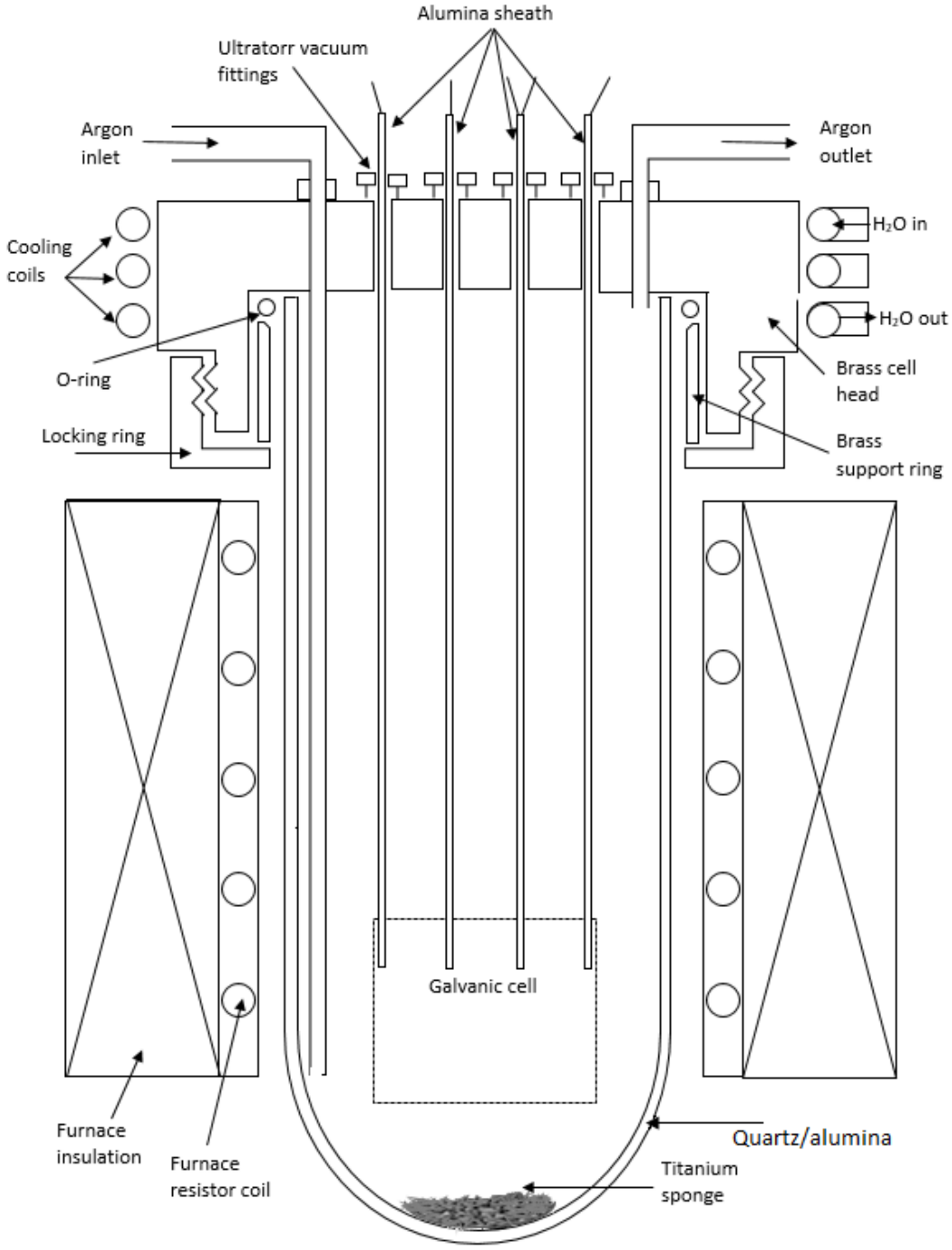

Figure 2. Schematic of the high-temperature measurement system for galvanic cell experiments.

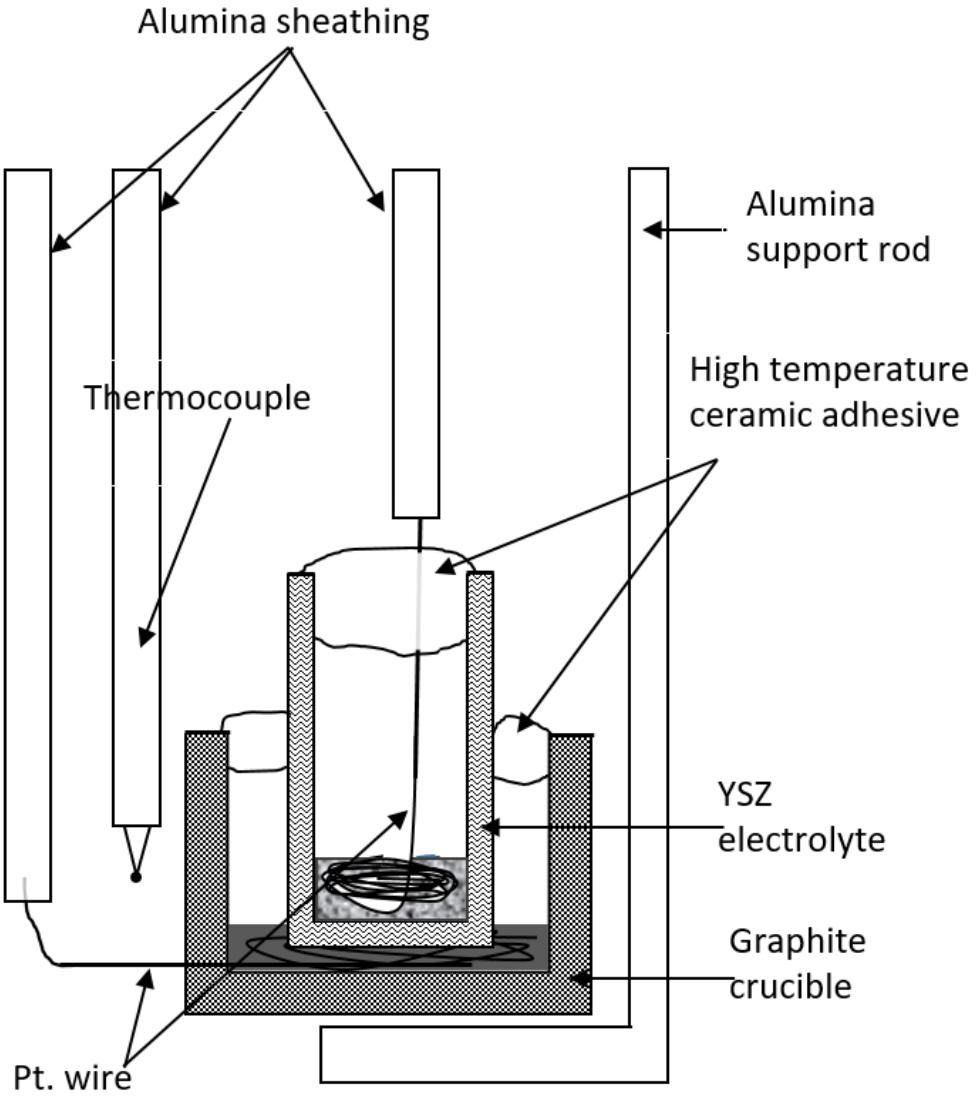

Figure 3. Open cell arrangement for Gibbs energy measurement.

3. RESULTS AND DISCUSSION

The temperature-related nature and general stability behavior of $CuGaSe_2$ measurements showed similarities with those in previous $CuInSe_2$ experiments [10]. Larger thermal fluctuations in cell temperature and longer equilibrium arrival times of EMF readings were more evident above 800 °C. In the temperature range of the experiments, $Cu+CuGaSe_2$ coexistence as a product of half-cell reactions was assumed. However, there is no phase diagram or stability information on the $Cu-CuGaSe_2$ system except for the Cu-Ga-Se solid-liquid phase diagram assessment at 1000 °C. Analogous to $CuInSe_2$ ternary phase relations, Mikkelsen [8] reports rapid diffusion of Cu in two-phase mixtures of Cu_2Se and $CuGaSe_2$ at 970 °C, although his data at 1000 °C (1273 K) show no coexistence or equilibrium between the two phases. The pseudobinary $Cu_2Se–Ga_2Se_3$ phase diagram [8] shows that $Cu_2Se+CuGaSe_2$ coexist up to 970 ºC. Furthermore, Cu-Se and Cu-Ga phase diagrams indicate that Cu is stable with

corresponding binaries up to 1000 ºC. Cu-$CuInSe_2$ phase equilibria reveal stable two phase coexistence up to 600 °C (873 K). Therefore, Cu-$CuGaSe_2$ coexistence in the measurement range is assumed.

The EMF results of three independent series of measurements are listed in Table 1. A linear regression line is plotted in Fig. 4. The least-squares expression of EMF over the range of 818-950 K is calculated as:

$$(EMF \pm 1.4)\ (mV) = 358.19 - 0.2117\ T\ (K) \quad (1)$$

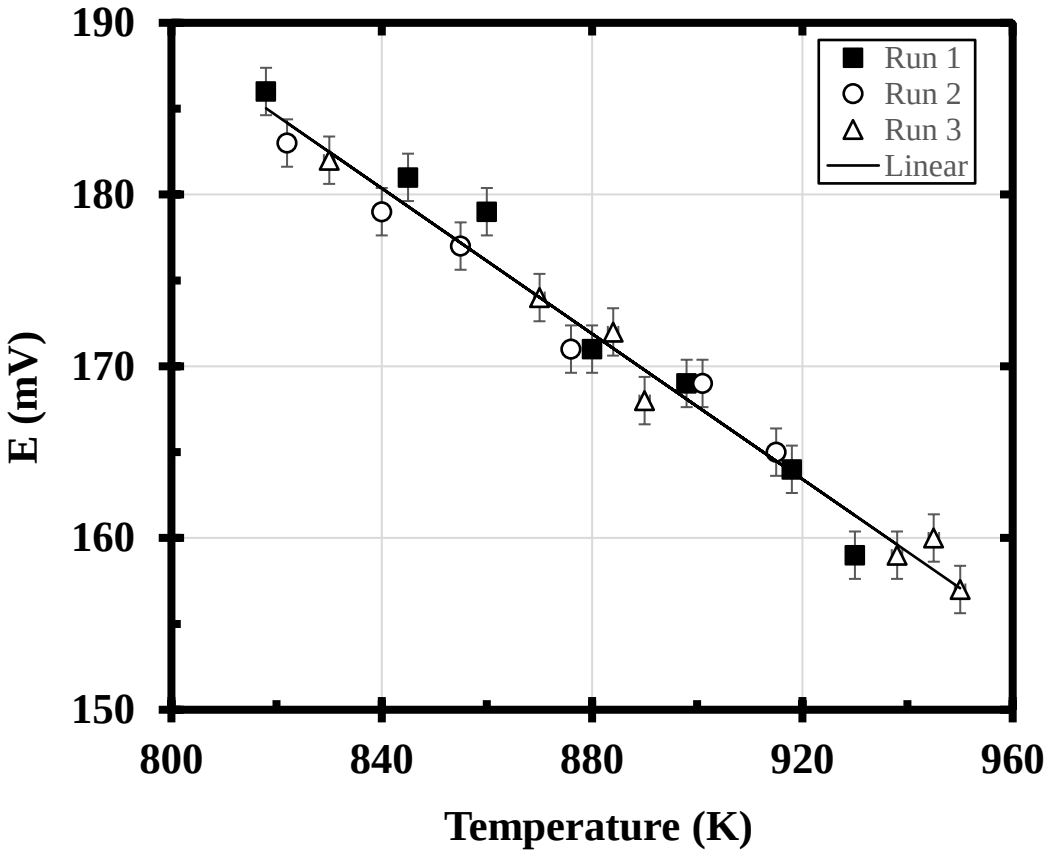

Figure 4. Linear regression of EMF data.

The two half-cell reactions of the cell can be represented as:

$$Ga(l) + 3/2O^{2-} \leftrightarrow \tfrac{1}{2}Ga_2O_3(s) + 3e^{-1} \quad (2a)$$

$$\tfrac{1}{2}\ Ga_2O_3(s) + 2Cu_2Se(ss) + 3e^{-1} \leftrightarrow CuGaSe_2(s) + 3Cu(s) + 3/2\ O^{2-} \quad (2b)$$

For the passage of three equivalent charges per mole of the ternary compound, the overall cell reaction can be represented as:

$$2Cu_2Se(ss) + Ga(l) \leftrightarrow CuGaSe_2(s) + 3Cu(s) \quad (3)$$

Thus, the standard Gibbs energy change for reaction ΔG_R in Equation (3) yields the following expression:

$$\Delta G_R = \Delta G^o_f(CuGaSe_2,s) - 2\ \Delta G^o_f(Cu_2Se,ss) \quad (4)$$

The Gibbs energy change of the overall reaction can be related to the measured cell EMF with the Nernst equation as:

ΔG_R (J/mol)= -nFE (5)

where F is Faraday's constant (96485.3415 C/mol), E is the open circuit potential in volts and n is the mole number of equivalent charges transferred per mole of ternary $CuGaSe_2$ in Equation (3). ΔG_R is calculated in the temperature range of 818-950 K as follows:

ΔG_R (kJ/mol)= -103.68 + 0.0613 T(K) (818 - 950 K) (6)

The Gibbs energy of formation of $CuGaSe_2$ can be calculated by substituting the calculated ΔG_R and Gibbs energy of formation for β-$Cu_{2-x}Se$ in Equation 4. However, the Gibbs energy function of β-$Cu_{2-x}Se$ is controversial even though the Cu-Se phase diagram has been relatively well studied.

3.1. Gibbs energy of Cu_2Se

β-$Cu_{2-x}Se$ is a relatively large homogeneous compound with a complex defect structure. Gibbs energy function assessments from phase diagram optimizations seem to vary depending on specific defect and liquid models along with uncertainty in homogeneity limits. The Cu-Se system was recently optimized by Chang [24]. All the compounds except Cu_2Se are reported as being stoichiometric in composition with a negligible homogeneity range. The homogeneity range of β-$Cu_{2-x}Se$ at room temperature was reviewed by Chakrabarti and Laughlin [25] and reported to be between approximately 35.4 and 36.0 at.% Se, corresponding to $0.18 \leq x$ in $Cu_{2-x}Se \leq 0.22$. The homogeneity range is evidently increased further at higher temperatures. Lorenz and Wagner [26] observed an extension of the $Cu_{2-x}Se$ phase field to a Cu/Se ratio less than 1.86 (>35 at. Se) at 673 K by coulometric titration. Furthermore, they estimated the composition of the copper-rich boundary for β-$Cu_{2-x}Se$ at 673 K, which is $Cu_{1.9975}Se$, by interpreting their experimental results using classical statistics. The homogeneity range of fcc β-$Cu_{2-x}Se$ was also reported by Singh and Bhan [27] and Stevels and Jellinek [28] as $0.15 \leq x$ in $Cu_{2-x}Se \leq 0.2$ at room temperature. Several researchers have suggested the existence of the two-phase region, α-$Cu_{2-x}Se$ and β-$Cu_{2-x}Se$, below 300 K; however, the higher temperature homogeneity limits for β-$Cu_{2-x}Se$ are not well studied. Frangis et al. [29] reported the α to β-$Cu_{2-x}Se$ transition temperature as ±40010 K and suggested a new γ phase when β-$Cu_{2-x}Se$ was quenched to liquid nitrogen temperature.

The thermodynamic data $\Delta H^o_{f,298}$ and S^o_{298} of Cu_2Se, CuSe and $CuSe_2$ were studied by Rau and Rabenau [30] using vapor pressure measurements. Additionally, there are a number of reports available on the enthalpy and entropy of formation of Cu-Se compounds mainly based on calorimetric [31], [32], [33], thermal analysis [34], and EMF methods [35]. There was also an assessment by K.C. Mills [36]. These results, however, show that there is a considerable discrepancy in the enthalpy and entropy of formation data for the binary compound Cu_2Se.

The most exhaustive list of thermodynamic and phase diagram data is summarized in the recent assessment by Chang [24]. According to the optimized phase diagram by Chang [24], the homogeneity range slightly narrows above 650 K. The β-$Cu_{2-x}Se$ compound is reported to be stable up to 1370 K with two phase coexistence with the Cu(fcc) solid phase for the copper-rich side of the phase diagram.

A recent value of the Gibbs energy function of Cu_2Se(ss) was derived in CIS assessment for phase diagram calculations by Ider [10]. This function was obtained from reassessment work by Shen, J. Y. (private communication). The calculated Gibbs energy of formation for the solid solution phase of

the β-$Cu_{2-x}Se$(ss) equation, (ΔG^o_f Cu_2Se,ss) (kJ/mol)=-0,024695T (K) - 60,698, seems to be significantly different from the Cu_2Se stoichiometric compound reported by Barin and Knacke [36]. The most recent data assessment was performed by Ider [38]. The calculated expression, (ΔG^o_f Cu_2Se,ss) (kJ/mol)= -63.02 - 0.0295 T (K), shows only a small discrepancy from stoichiometric compound data from Barin and Knacke [36]. A third law analysis showed that the value of $\Delta H^o_{f,298}$ = -65.81 kJ mol^{-1} also agrees with the value of -65.27 kJ mol^{-1} from Barin and Knacke [36]. However, many optimization and defect modeling studies show discrepancies in enthalpy and Gibbs energy functions. Hence, the Gibbs energy of formation for Cu_2Se as a line compound from Barin and Knacke [36] is assumed in this calculation.

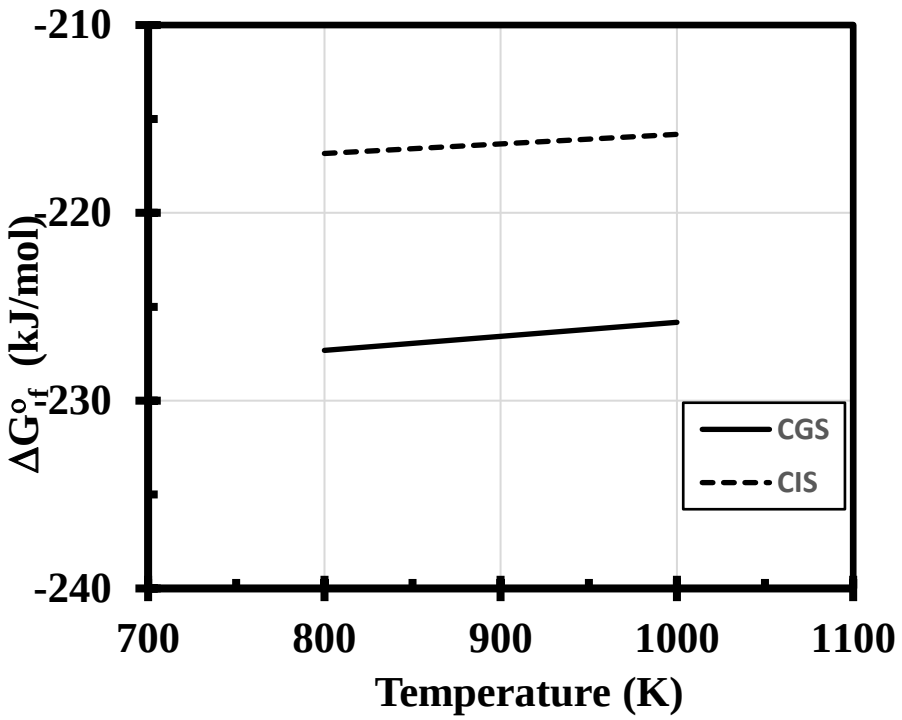

Figure 5. Standard Gibbs energy of formation of Cu(In, Ga)Se_2 compounds.

The following function for Cu_2Se from Barin and Knacke [36] between 600 – 1000 K is derived by interpolation.

(ΔG^o_f Cu_2Se,ss) (kJ/mol)= -64.813 - 0.0269 T (K) (600 - 1000 K) (7)

Substituting Equations (6) and (7) in Equation (4), the following expression for the standard Gibbs energy of formation of $CuGaSe_2$ is obtained:

(ΔG^o_f $CuGaSe_2$) (kJ/mol)= -233.31 + 0.0075 T (K) (818 - 950 K) (8)

Similarly, the stability of $CuInSe_2$ using the coexisting mixture Cu_2Se / $CuInSe_2$ / Cu / In_2O_3 was measured before by Ider [10]. Furthermore, the phase relations for the pseudobinary line for Cu_2Se-In_2Se_3 were optimized, and the Gibbs energy of the formation functions for α and δ-$CuInSe_2$ was calculated from the measured data as follows:

ΔG^o_f α-$CuInSe_2$) (kJ/mol)= -220.92 + 0.0051 T (K) (949-1044 K) (9)

ΔG^o_f δ-$CuInSe_2$) (kJ/mol)= -210.92 - 0.0043 T (K) (1055-1150 K) (10)

A comparison is made in Table 2 of the ΔG^{o}_{f} of α-$CuInSe_2$ and $CuGaSe_2$. The same set of data plotted in Fig. 5 shows the slight slope difference.

The formation of $CuGaSe_2$ from elements in their standard states can be represented as:

$$Cu(s) + 2Se(s,l) + Ga(s,l) \leftrightarrow CuGaSe_2(s) \quad (11)$$

The Gibbs energy G-H^{SER} function is regularly needed for data assessment and phase diagram calculations. The term SER represents the standard element reference. The Gibbs energy change of the reaction in Equation 11 is the same as the stoichiometric difference between the Gibbs energy functions of $CuGaSe_2$ and the elements.

By using the ΔG^{o}_{f} $CuGaSe_2$ and Gibbs energy functions of elements, the Gibbs energy function of $CuGaSe_2$ is calculated in the temperature range of 818 - 950 K as:

$$(G_{CuGaSe_2}) = \text{-0.319 T (K) -146.65 kJ/mol} \quad (818 - 950\ K) \quad (12)$$

For Equation 12, the Gibbs energy functions for the elements in their most stable forms are obtained from the FactSageEdu database [39]. The Gibbs energy function parameters with temperature ranges are presented in Table 4. The calculated Gibbs energy expression is given relative to the reference state of 298 K at which the Gibbs formation energies of elements are taken as zero. The expressions for pure elements are calculated by using curve fit parameters in the temperature range of the measurements.

The ΔG^{o}_{f} values at 1000 K show that the ternary $CuGaSe_2$ compound is slightly more stable than the $CuInSe_2$ compound (10 kJ/mol), which is consistent with our recent phase diagram optimization studies. Since there are few data published on the Gibbs energy of the $CuGaSe_2$ compound, a comparison with other data cannot be made.

No third-law analysis could be carried out due to the lack of reliable S^{o}_{298} and C^{o}_{P} data on $CuGaSe_2$. Berger [40] determined values of 316.7 kJ/mol and 267.4 kJ/mol for $\Delta H^{o}_{f,298}$ of $CuGaSe_2$ and $CuInSe_2$ by mass spectrometry. Additionally, Glazov [14] estimated the values of $\Delta H^{o}_{f,298}$ of both ternary compounds by using a modified version of the two equations mentioned in [41]. Cahen [21] calculated $\Delta G^{o}_{f,298}$ of $CuGaSe_2$ and $CuInSe_2$ from the available literature according to the formation reactions from binary chalcogenides. Cahen [21] also reported limited experimental data and theoretically calculated free energies and enthalpies of formation for $CuInSe_2$ and $CuGaSe_2$. These values are compared in Table 3.

Table 1. EMF data for galvanic **cells.**

Run	T (K)	E (mV)	T (K)	E (mV)
1	818	186	930	159
	845	181	918	164
	860	179	898	169
	880	171		
2	822	183	915	165
	840	179	901	169
	855	177	876	171
3	938	159	890	168
	870	174	945	160
	830	182	950	157
	884	172		

Table 2. ΔG^o_f for ternary compounds of $CuInSe_2$ and $CuGaSe_2$.

Compounds	ΔG^o_f (kJ/mol) [A+BT (K)]		T Range (K)	ΔG^o_f (kJ/mol)	Ref
	A	B		(1000 K)	
α-$CuInSe_2$	-218.05	0.0439	949-1044	-174.15	[42]
	-220.92	0.0051	949-1044	-215.82	[10]
$CuGaSe_2$	-224.67	0.0422	818-1053	-182.51	[42]
	-233.31	0.0075	818-950	-225.81	This Work

Table 3. Comparison of $\Delta H^o_{f,298}$ and $\Delta G^o_{f,298}$ for $CuGaSe_2$ and $CuInSe_2$.

Solid Phase	Method	$-\Delta H^o_{f,298}$ (kJ/mol)	Reference	$-\Delta G^o_{f,298}$ (kJ/mol)	Reference
$CuGaSe_2$	Mass Spectrometry	316.7	[40]		
	Calculated	324.7	[41]	313	[21]
	Calculated	295.8	[41]		
	Calculated	326	[21]		
	Calculated	249	[21]		
$CuInSe_2$	Mass Spectrometry	267.4	[40]		
	EMF	202.9	[10]		
	Calculated	260.2	[41]		
	Calculated	268.6	[41]		
	Calculated	308.0	[21]	262	[21]
	Calculated	201	[21]	201	[21]

Table 4. Gibbs energy functions for elements [39] in J/mol for 1 bar.

Coefficient	G, J/mol, 1 bar $G = A + BT + CT^2 + DT^{-1} + ET^3 + Fln(T) + GTln(T) + HT^{-2}$		
	Cu, solid (298-1100K)	Ga, liquid (303-3000K)	Se, liquid (494-1000K)
A	4202.903490	-2295.65181	-10110.787
B	197.366194	118.648473	289.505559
C	$4.565823899*10^{-3}$	$7.412438567*10^{-6}$	$2.4883*10^{-2}$
D	- 106313.403	68793.1928	0
E	$-1.144561123*10^{-6}$	0	$-5.434666667*10^{-6}$
F	– 2799.24538	0	0
G	– 33.5575315	-26.6221078	-52.408
H	0	-15529672.3	0

4. CONCLUSION

Solid-state EMF experiments were performed in the Cu-Ga-Se system to measure the Gibbs energy of formation of $CuGaSe_2$. Experimental studies and literature data have been assessed and compared with a previous assessment of the $CuInSe_2$ system. A comparison is made on the Gibbs energy of the formation functions of $CuInSe_2$ and $CuGaSe_2$. It was found that the standard molar entropy of formation values were of similar order. The nearly equal slopes of In and Ga ternaries can also be readily seen from Fig. 5. The ΔG^o_f values at 1000 K showed that the ternary $CuGaSe_2$ compound is slightly more stable than the $CuInSe_2$ compound, which is consistent with the current phase diagram information.

NOMENCLATURE

15 YSZ	: 8 mole % yittria (Y_2O_3) stabilized zirconia (ZrO_2), $(ZrO_2)_{0.92}(Y_2O_3)_{0.08}$
EMF, E	: electromotive force (volt), E
Pt. (wire)	: platinum (wire)
eV	: electron volt, $1.602176634 \cdot 10^{-19}$ Joules
Å	: angstrom, 10^{-10} m
ε	: ε-$Cu_1Ga_5Se_8$
δ	: δ-$Cu_1Ga_3Se_5$
γ	: γ-$Cu_xGa_ySe_z$ compound stable between 0.6-0.7 mole% Ga_2Se_3 in Cu_2Se- Ga_2Se_3 phase line.
Zb	: zinc blende crystal structure
I-III-VI_2	: group 1B (Cu, Ag) – group 3A (Ga, In) – group 6A (S, Se, Te)
KBr	: potassium bromide
Alumina	: aluminum oxide, Al_2O_3
Quartz	: SiO_2 oxide mineral
ΔG_R	: Gibbs energy change of a reaction, J/mol
n	: number of moles of electrons exchanged in electrochemical reaction
F	: Faradays constant, 96485.332 coulomb/mole
β-$Cu_{2-x}Se$	: near stoichiometric stable compound between 300K-1400K
ss, (ss)	: solid solution
α-CIS	: α-$CuInSe_2$, chalcopyrite $CuInSe_2$
δ-CIS	: δ-$CuInSe_2$, sphalerite $CuInSe_2$
C^0_p	: heat capacity, Joules/kelvin
S^0_{298}	: standard molar entropy at 298 K

References

1. S. Prabahar, V. Balasubramanian, N. Suryanarayanan and N. Muthukumarasamy, *Chalcogenide Lett.,* 7 (2010) 49.
2. S.R. Kodigala, Thin Films and Nanostructures; $Cu(In_{1-x}Ga_x)Se_2$ Based Thin Film Solar Cells, Academic Press, (2010) Burlington, MA, USA.
3. J.L. Shay, B. Tell, H.M. Kasper and L.M. Schiavone, 1972. *Phys. Rev. B*, 5 (1972) 5003.
4. T. Tinoco, C. Rincón, M. Quintero and G.S. Pérez, *Phys. Status Solidi A,* 124 (1991) 427.
5. K.J. Bachmann, M.L. Fearheiley, Y.H. Shing and N. Tran, *Appl. Phys. Lett.,* 44 (1984) 407.
6. L.L. Kazmerski, F.R. White and G.K. Morgan, *Appl. Phys. Lett.*, 29 (1976) 268.
7. H. Hahn, G. Frank, W. Klinger, A.D. Meyer and G. Störger, *Z. Anorg. Allg. Chem,* 271 (1953) 153.
8. J.C. Mikkelsen, *J. Electron. Mater*, 10 (1981) 541.
9. L.S. Palatnik and E.K. Belova, *Izv. Akad. Nauk SSSR, Neorg. Mater.,* 3 (1967) 2194.
10. M. Ider, R. Pankajavalli, W. Zhuang, J.Y. Shen and T.J. Anderson, *J. Alloys Compd.* 604 (2014) 363.
11. S. Lehmann, Ph.D. Thesis, FreieUniversit¨at Berlin, (2007).
12. A. Meeder, L. Weinhardt, R. Stresing, D. Fuertes Marrón, R. Würz, S.M. Babu, T. Schedel-Niedrig, M.Ch. Lux-Steiner, C. Heske and E. Umbach, *J. Phys. Chem. Solids,* 64 (2003) 1553.
13. S.M. Wasim, C. Rinco´n, G. Marin and J. M. Delgado, *Appl. Phys. Lett.,* 77 (2000) 94.
14. V.M. Glazov, V.V. Lebedev, A. D. Molodyk and A. S. Pashinkin, *Inorg. Mater.*, 15 (1979) 1469.
15. I.V. Bodnar and A.P. Bologa, *Cryst. Res. Technol.,* 17 (1982) 339.
16. L.S. Palatnik and E. I. Rogacheva, *Izv. Akad. Nauk SSSR, Neorg. Mater.*, 2 (1966) 659.
17. H. Jitsukawa, H. Matsushita and T. Takizawa., *J. Cryst. Growth,* 186 (1998) 587.
18. H. Matsushita, H. Jitsukawa and T. Takizawa., *J. Cryst. Growth*, 166 (1996) 712.
19. T. Tanaka, Y. Demizu and A. Yoshida, *J. Appl. Phys.*, 81 (1997) 7619.
20. D.J. Schroeder, J.L. Hernandez, G.D. Berry and A.A. Rockett, *J. Appl. Phys.,* 83 (1998) 1519.
21. D. Cahen and R. Noufi, *J. Phys. Chem. Solids*, 53 (1992) 991.
22. T.J. Anderson and L.F. Donaghey, *J. Chem. Thermodyn.*, 9 (1977) 603.
23. T.J. Anderson, T.L. Aselage and L.F. Donaghey,, *J. Chem. Thermodyn.*, 15 (1983) 927.
24. C.-H. Chang, Ph. D. Thesis, University of Florida, (1999).
25. D.J. Chakrabarti and D.E. Laughlin, *Bull. Alloy Phase Diagrams,* 2 (1981) 305.
26. G. Lorenz and C. Wagner, *J. Chem. Phys.*, 26 (1957) 1607.
27. M. Singh and S. Bhan, *Prog. Cryst. Growth Charact. Mater.*, 20 (1990) 217.
28. A.L.N. Stevels and J. Jellinek, *Recl. Trav. Chim. Pays-Bas,* 90 (1971) 273.
29. N. Frangis, C. Manolikas and S. Amelinckx, *Phys. Status Solidi A,* 126 (1991) 9.
30. H. Rau and A. Rabenau, *J. Solid State Chem.*, 1 (1970) 515.
31. G. Gattow and A. Schneider, *Z. Anorg. Allg. Chem.*, 286 (1956) 296.
32. P. Kubaschewski and J. Nölting, *Ber. Bunsen Ges. Phys. Chem.,* 77 (1973) 70.
33. R. Blachnik and P.-G. Gunia, Z. *Naturforsch., A: Phys. Sci.,* 33 (1978) 190.
34. R. Murray and R.D. Heyding, *Can. J. Chem.*, 53 (1975) 878.
35. K. Askerova, N.A. Alieva, T.R. Azizov, A.S. Abbasov, F.M. Mustafayev, *Izv. Akad. Nauk Azerb. SSR*, 6 (1976) 137.
36. K.C. Mills, Thermodynamic Data for Inorganic Sulphides, Selenides and Tellurides. Butterworths, (1974) London, UK.
37. I. Barin, O. Knacke and O. Kubaschewski, Thermochemical Properties of Inorganic Substances, Springer-Verlag, (1973) Berlin.
38. M. Ider, *Solid State Ionics*, 329 (2019) 140.
39. C.W. Bale, E. Bélisle, P. Chartrand, S.A. Decterov, G. Eriksson, A.E. Gheribi, K. Hack, I.H. Jung, Y.B. Kang, J. Melançon, A.D. Pelton, S. Petersen, C. Robelin. J. Sangster, P. Spencer and M-A. Van Ende, FactSage Thermochemical Software and Databases - 2010 - 2016, *Calphad*, 54 (2016) 35.
40. L.I. Berger, S.A. Bondar, V.V. Lebedev, A.D. Molodyk and S.S. Strel'Chenko, *Nauk. I Tekhnika*,

(1973) 248.
41. J.C. Phillips and J.A. Van Vechten, *Phys. Rev. B,* 2 (1970) 2147.
42. M. Ider, Ph. D. Thesis, University of Florida, (2003).